

Grain growth and dislocation density evolution in a nanocrystalline Ni–Fe alloy induced by high-pressure torsion

S. Ni,^a Y.B. Wang,^a X.Z. Liao,^{a,*} S.N. Alhajeri,^b H.Q. Li,^c Y.H. Zhao,^d E.J. Lavernia,^d S.P. Ringer,^e T.G. Langdon^{f,g} and Y.T. Zhu^h

^aSchool of Aerospace, Mechanical and Mechatronic Engineering, The University of Sydney, Sydney, NSW 2006, Australia

^bDepartment of Manufacturing Engineering, College of Technological Studies, PAAET, Shuwaikh 70654, Kuwait

^cLos Alamos National Laboratory, Los Alamos, NM 87545, USA

^dDepartment of Chemical Engineering and Materials Science, University of California, Davis, CA 95616, USA

^eAustralian Centre for Microscopy & Microanalysis, The University of Sydney, NSW 2006, Australia

^fDepartments of Aerospace & Mechanical Engineering and Materials Science, University of Southern California, Los Angeles, CA 90089-1453, USA

^gMaterials Research Group, School of Engineering Sciences, University of Southampton, Southampton SO17 1BJ, UK

^hDepartment of Materials Science & Engineering, North Carolina State University, Raleigh, NC 27659-7919, USA

Received 27 September 2010; revised 18 October 2010; accepted 20 October 2010

Available online 26 October 2010

The structural evolution of a nanocrystalline Ni–Fe alloy induced by high-pressure torsion (HPT) was investigated. HPT-induced grain growth occurred via grain rotation and coalescence, forming three-dimensional small-angle sub-grain boundaries. Further deformation eliminates the sub-grain boundaries from which dislocations glide away on different {1 1 1} planes. A significant number of these dislocations come together to form Lomer–Cottrell locks that effectively increase the dislocation storage capacity of the nanocrystalline material. These observations may help with developing strong and ductile nanocrystalline materials.

© 2010 Acta Materialia Inc. Published by Elsevier Ltd. All rights reserved.

Keywords: Severe plastic deformation; Nanocrystalline materials; Dislocation density; High-pressure torsion

Ultrafine-grained (UFG, <1 μm) and nanocrystalline (nc, <100 nm) materials present significantly higher yield strength than their coarse-grained counterparts due to the Hall–Petch effect [1,2]. However, the high yield strength is usually achieved at the expense of the ductility, and this can be exacerbated in nc alloys because of dimensional limitations imposed on the generation and storage of dislocations [1,2]. In particular, a fundamental reason for the low ductility of UFG and nc materials is the lack of strain hardening due to an inability to accumulate dislocations because of their small grain sizes and saturation of dislocations [2,3]. For example, unlike coarse-grained materials, in which dislocation densities increase with increasing strain [4], both molecular dynamics simulations [5] and experiments [3,6] suggest that plastic deformation normally does not increase the dislocation density in nc materials. These difficulties in simulta-

neously achieving high strength and good ductility in UFG and nc materials severely limit the practical applications of the materials.

In recent years, significant efforts have been made to improve the ductility of UFG and nc materials by restoring the work hardening or dislocation storage capacity within the materials through the introduction of bimodal or multi-modal microstructures [7,8], pre-existing growth twins [9], deformation twins [10,11], second phase precipitation [12,13] and phase transformations [14]. Many of these methods effectively improve the ductility without sacrificing the strength [7,10,11,13].

In a previous paper, we reported that severe plastic deformation (SPD) of an nc Ni–Fe alloy resulted in an increase in dislocation density [15]. This is important when considering the possibility of applying SPD to develop materials with exceptional strength and ductility. It is therefore important to understand the physical mechanism underlying the increase in the dislocation density in the nc material. It is well known that grain boundary (GB)-mediated deformation mechanisms,

* Corresponding author. Tel.: +61 2 9351 2348; fax: +61 2 9351 7060; e-mail addresses: xiaozhou.liao@sydney.edu.au; xliao@usyd.edu.au

such as grain rotation and GB sliding/migration, play a dominant role in nc materials [16]. This is indeed the case for the plastic deformation of the nc Fe–Ni alloy [15,17], in which deformation-induced grain growth via grain rotation and coalescence occurs during SPD. In this study, a detailed X-ray diffraction (XRD) and transmission electron microscopy (TEM) investigation was conducted in order to obtain an understanding of the relationship between grain growth processes and the changes in dislocation density of an nc Ni-20 wt.% Fe alloy. The results show that the grain growth mechanism has a significant effect on the evolution of the dislocation density. The three-dimensional small-angle sub-grain boundaries formed during the grain rotation process possess a high density of dislocations. Further deformation eliminates the sub-grain boundaries from which full dislocations glide away on different $\{111\}$ planes. As the grain size increases to ~ 50 nm, the dimensional limitations imposed on dislocation behavior in nc material are alleviated [18]. As a result, multiple slip systems are activated, resulting in strong dislocation interactions and the formation of Lomer–Cottrell (L–C) locks that effectively increase the dislocation storage capacity of the nc material. These observations indicate a dislocation behavior transition from one that operates in nc materials to one that occurs in coarse-grained materials when grain sizes reach ~ 50 nm.

The nc Ni-20 wt.% Fe alloy studied here was a non-equilibrium supersaturated solid solution with a single face-centred cubic (fcc) structure produced by electrochemical deposition [19]. The SPD was conducted with a quasi-constrained high-pressure torsion (HPT) facility [20] using discs with a diameter of ~ 10 mm and a thickness of ~ 0.8 mm. These discs were subjected to $1/4$ -revolution HPT under an applied pressure of 3 GPa and 2-, 5- and 10-revolution HPT under an applied pressure of 6 GPa using a rotation rate of 1 rpm. Although local shear strain turbulence may exist during HPT processing [21], the equivalent strain, ε , in HPT is generally defined as $\varepsilon = \frac{2\pi Nr}{\sqrt{3}h}$, where r is the distance from the disc centre, h is the thickness of the disc and N is the number of HPT revolutions [20]. This relationship will be used for convenience in the discussions in this paper.

The XRD measurements were performed using a Siemens D5000 X-ray diffractometer on the central part ($d < 2.5$ mm) and the edge part ($2.5 \text{ mm} < d < 5$ mm) of each disc. XRD peak broadening was used to evaluate the crystalline grain size d_{XRD} and microstrain $\langle \varepsilon^2 \rangle^{1/2}$ using the Williamson–Hall integral-breadth method [22]. The dislocation density, ρ , was estimated from the simple approach of Williamson and Smallman [23] and Smallman and Westmacott [24] using the following relationship: $\rho = \frac{2\sqrt{3}\langle \varepsilon^2 \rangle^{1/2}}{d_{\text{XRD}}b}$, where b is the absolute value of the Burgers vector ($\frac{1}{2}\langle 110 \rangle$) of a full dislocation in the fcc Ni–Fe alloy. The errors in these dislocation density measurements were assessed by scanning each specimen three times and were demonstrated to be less than 6%, which is significantly smaller than the dislocation density changes between different deformation stages.

Samples for TEM were prepared via standard techniques [17] and experiments were performed using a JEOL JEM-3000F operating at 300 kV. The average

grain sizes were statistically estimated by measuring at least 200 grains with clear grain boundaries in bright-field TEM images where the grains exhibit strong diffraction conditions and therefore appear dark.

Based on the hardness evolution of HPT discs as a function of imposed shear strain, which will be discussed elsewhere because of the space limit of this paper, the HPT deformation process is divided into stages I, II, III and IV, which correspond to the equivalent strain regions of 0–4.5, 4.5–20, 20–35 and 35–182, respectively. The TEM measurements indicated that the average grain sizes in these four stages were 22, 30, 35 and 50 nm consecutively, revealing continuous grain growth with increasing strain. Figure 1 provides typical low-magnification TEM images of (a) the as-deposited material and (b) the edge part of the 10-revolution HPT disc, which corresponds to the region subjected to the largest plastic strain. A uniform microstructure is observed in the as-deposited material with an initial average grain size of ~ 21 nm. Figure 1b is evidence of significant grain growth after HPT for 10 revolutions. A previous detailed TEM investigation on a similar material indicates that the grain growth occurred via grain rotation and coalescence [17].

The XRD analysis was conducted for the as-deposited material and HPT samples in the four deformation stages. As shown in Figure 2a, all XRD diffraction peaks were indexed based on the fcc Ni structure, indicating that the HPT process did not introduce any phase transformation. Dislocation densities calculated from the XRD peak broadening and the average grain sizes measured from TEM images at the four deformation stages are summarized in Figure 2b. The average dislocation density of the as-deposited material was $2.2 \times 10^{15} \text{ m}^{-2}$ and this increased to $3.6 \times 10^{15} \text{ m}^{-2}$ at deformation stage I. The average dislocation density reached a plateau of $5.8 \times 10^{15} \text{ m}^{-2}$ at deformation stage II, but dropped sharply to $4.1 \times 10^{15} \text{ m}^{-2}$ at stage III, which has a relatively narrow range of equivalent strain values of ~ 20 –35. It is noted that the dislocation density at the location where there exists an equivalent strain of ~ 35 may be close to that of the as-deposited material because of the equivalence in hardness measurements (not shown here), but this speculation is difficult to confirm experimentally due to the difficulty of conducting XRD on very small amounts of material. The dislocation density

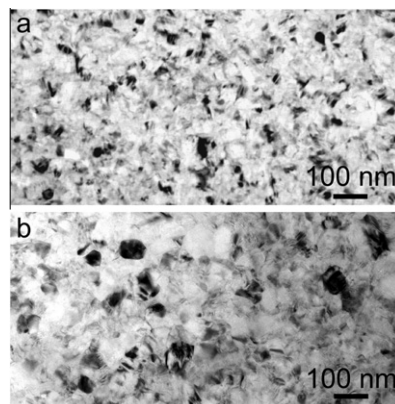


Figure 1. Typical low-magnification TEM images of the as-deposited material (a) and the edge of the 10-revolution HPT disc (b).

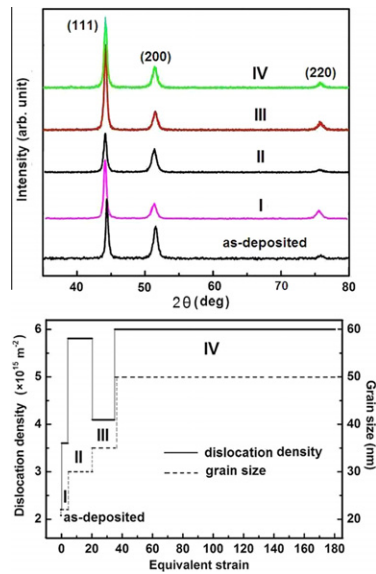


Figure 2. (a) XRD patterns obtained from the as-deposited material and materials with deformation stages (I–IV). (b) Deformation stages, average grain sizes and dislocation densities as functions of equivalent HPT shear strain.

increased again with further deformation, reaching the second plateau of $\sim 6.0 \times 10^{15} \text{ m}^{-2}$ at stage IV.

Whereas the XRD data provide global information on the average dislocation density, high-resolution TEM images present local information on the spatial distribution of the dislocations. Detailed TEM investigations revealed that the dislocations were distributed randomly throughout grains at stages I, II and III. A typical $\langle 110 \rangle$ zone-axis high-resolution TEM image from a single grain at deformation stage III is provided in Figure 3a and the enlarged Fourier-filtered image in Figure 3b was recorded from the region within the white square in Figure 3a. Cores of dislocations are indicated by white “T” in Figure 3b. By contrast, a typical high-resolution TEM image of a grain at stage IV is provided in Figure 3c and its enlarged Fourier-filtered image in Figure 3d was recorded within the white square in Figure 3c. These images show that groups of closely positioned dislocations are visible in deformation stage IV, clearly indicating that dislocation reactions and/or tangling occur at this stage.

For nc grains with grain sizes $< 50 \text{ nm}$, grain boundaries usually act as dislocation sources and sinks [25] so that dislocations form at one grain boundary segment and glide through the grains to disappear at another grain boundary segment on the other side of the grain. The present experimental results suggest that a high density of dislocation sources exists at the grain boundaries of the as-deposited sample. Therefore, the rate of dislocation generation is relatively high in the initial stages of deformation in the strain region of 0–20. The rise in the dislocation density in the initial stage of plastic deformation indicates that the rate of dislocation generation is higher than the rate of dislocation annihilation.

As predicted on the basis of molecular dynamics simulations [26], a high density of dislocations within nc grains is very unstable and the dislocations tend to glide towards, and disappear at, the grain boundaries when

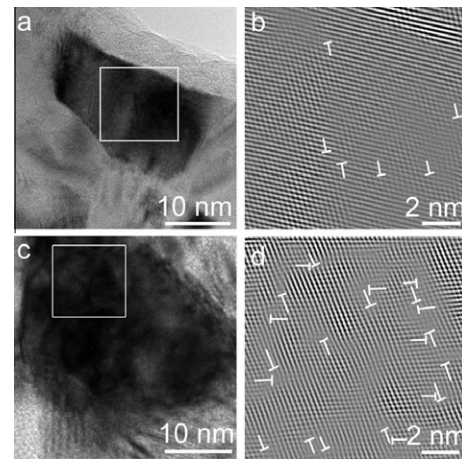


Figure 3. Typical high-resolution TEM images of grains at deformation stages III and IV and their corresponding Fourier-filtered images obtained from the areas marked by white squares: dislocations are indicated with white “T”. (a) and (b) are from deformation stage III, (c) and (d) from deformation stage IV.

an external force is available to activate dislocation slip [27]. This seems to be the case in the Ni–Fe alloy studied here. Further deformation of the material forces the dislocations, which are initially weakly pinned by solute atoms, to disappear at the grain boundaries. The dislocation density reduction seen in deformation stage III suggests that the rate of dislocation disappearance at grain boundaries surpassed that of dislocation generation, indicating a reduction in dislocation sources at grain boundaries with continuing deformation. This result is consistent with the report that each dislocation source at GBs operates only once and therefore the amount of dislocation sources is reduced with continuing deformation [18].

Consistent with previous observations [15,17], the deformation process resulted in grain growth via grain rotation and the formation of larger grains containing high fractions of low-angle sub-grain boundaries with high densities of misfit dislocations located at these sub-grain boundaries [15]. With further development of HPT processing, the misorientation angles between neighbouring sub-grains decrease gradually to zero and the dislocations that accommodate the misorientation necessarily glide away [15,28]. This results in grain growth to $\sim 50 \text{ nm}$ and the activation of multiple slip on different $\{111\}$ planes because of the alleviation of dimensional limitations imposed on dislocation behavior in nc grains [18]. The sub-grain boundary dislocations, which exist three-dimensionally [15] and slip on different $\{111\}$ planes, may meet, interact and tangle with each other, increasing the dislocation density in the material, as is evident in the TEM image in Figure 3d. The experimental results indicate a transformation of dislocation behavior from one that operates in nc materials to one in coarse-grained materials when the grain sizes reach $\sim 50 \text{ nm}$.

It has been reported that the existence of a high density of dislocations on two inter-crossing $\{111\}$ planes provides a high probability for the formation of Lomer–Cottrell locks, each of which is formed by the reaction of two leading partials from two dissociated lattice dislocations on two intersecting slip planes [29]. Figure 4

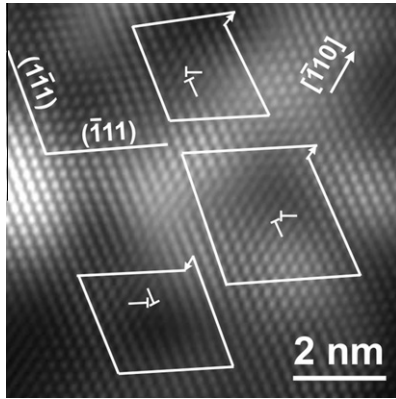


Figure 4. A typical Fourier-filtered high-resolution TEM image showing the formation of L–C locks at deformation stage IV: Burgers circuits are drawn in the image.

shows a typical high-resolution TEM image that provides evidence of L–C lock formation at deformation stage IV. Noting that the image in Figure 4 was recorded along the $[1\ 1\ 0]$ direction, the two $\{1\ 1\ 1\}$ plane groups in the image can be indexed as $(1\bar{1}\bar{1})$ and $(\bar{1}11)$, respectively, and the $\langle 1\ 1\ 0 \rangle$ direction indicated in Figure 4 is $[1\bar{1}0]$. It should be noted also that a lattice dislocation in an fcc metal is normally dissociated into two $1/6\langle 1\ 1\ 2 \rangle$ type partial dislocations. For example, a lattice dislocation with the Burgers vector of $\frac{1}{2}[0\bar{1}1]$ on $(1\bar{1}\bar{1})$ is dissociated into $\frac{1}{6}[\bar{1}\bar{1}\bar{2}] + \frac{1}{6}[\bar{1}\bar{2}\bar{1}]$ and a lattice dislocation with the Burgers vector of $\frac{1}{2}[101]$ on $(\bar{1}11)$ is dissociated into $\frac{1}{6}[211] + \frac{1}{6}[\bar{1}\bar{1}\bar{2}]$. When the two lattice dislocations meet at an intersection of the $(1\bar{1}\bar{1})$ and $(\bar{1}11)$, the two leading partials interact and form a stair-rod dislocation $\frac{1}{6}[\bar{1}\bar{2}\bar{1}] + \frac{1}{6}[211] \rightarrow \frac{1}{6}[1\bar{1}0]$. Together with the other two partial dislocations, this forms an L–C lock structure [29]. The overall Burgers vector of the L–C lock is $\frac{1}{2}[1\bar{1}0]$, which is clearly evident in Figure 4. Because the L–C lock structure is extended on two $\{111\}$ planes, it provides a strong barrier to dislocation glide [29] and leads to a significant accumulation of dislocations in the nc Ni–Fe alloy in stage IV. Note that reactions between different combinations of partials from two slip planes can lead to various types of stair-rod dislocations [29]. In this study, careful observations show that large numbers of dislocations lying on different $\{111\}$ planes are closely positioned at deformation stage IV, and many of these dislocations form L–C locks. The formation of a high density of L–C locks hinders the motion of dislocations severely, which increases the dislocation density and may contribute significantly to both strength and ductility.

In summary, the dislocation density decreases due to dimensional limitations of the nc material after reaching a saturation condition at the initial stages of deformation. The formation of large numbers of L–C locks, which is a direct consequence of the deformation-induced grain growth and the transition of dislocation behavior when grain sizes reach ~ 50 nm, is responsible for a subsequent increase in the dislocation density, which may increase significantly the dislocation storage capability and potentially help with achieving good ductility as well as strength in the material.

The authors are grateful for scientific and technical input and support from the Australian Microscopy & Microanalysis Research Facility node at the University of Sydney. This project is supported by the Australian Research Council (Grant No. DP0772880, to S.N., Y.B.W. and X.Z.L.), the LDRD program of Los Alamos National Laboratory (to H.Q.L.), the Office of Naval Research (Grant Nos. N00014-04-1-0370 and N00014-08-1-0405, to Y.H.Z. and E.J.L.), the National Science Foundation of the United States (Grant No. DMR-0855009, to T.G.L.) and the US Army Research Office and Army Research Laboratory (to Y.T.Z.). S.N. also appreciates support from the China Scholarship Council.

- [1] R.Z. Valiev, *Nature* 419 (2002) 887.
- [2] Y.T. Zhu, X.Z. Liao, *Nat. Mater.* 3 (2004) 351.
- [3] Z. Budrovic, H. Van Swygenhoven, P.M. Derlet, S.V. Petegem, B. Schmitt, *Science* 304 (2004) 273.
- [4] V.V. Stolyarov, Y.T. Zhu, I.V. Alexandrov, T.C. Lowe, R.Z. Valiev, *Mater. Sci. Eng. A* 343 (2003) 43.
- [5] V. Yamakov, D. Wolf, M. Salazar, S.R. Phillpot, H. Gleiter, *Acta Mater.* 49 (2001) 2713.
- [6] M. Legros, B.R. Elliott, M.N. Rittner, J.R. Weertman, K.J. Hemker, *Phil. Mag. A* 80 (2000) 1017.
- [7] Y. Wang, M. Chen, F. Zhou, E. Ma, *Nature* 419 (2002) 912.
- [8] Z. Lee, D.B. Witkin, V. Radmilovic, E.J. Lavernia, S.R. Nutt, *Mater. Sci. Eng. A* 410 (2005) 462.
- [9] L. Lu, Y. Shen, X. Chen, L. Qian, K. Lu, *Science* 304 (2004) 422.
- [10] Y.H. Zhao, Y.T. Zhu, X.Z. Liao, Z. Horita, T.G. Langdon, *Appl. Phys. Lett.* 89 (2006) 121906.
- [11] Y.H. Zhao, J.F. Bingert, X.Z. Liao, B.Z. Cui, K. Han, A. Sergueeva, A.K. Mukherjee, R.Z. Valiev, T.G. Langdon, Y.T. Zhu, *Adv. Mater.* 18 (2006) 2949.
- [12] Z. Horita, K. Ohashi, T. Fujita, K. Kaneko, T.G. Langdon, *Adv. Mater.* 17 (2005) 1599.
- [13] Y.H. Zhao, X.Z. Liao, S. Cheng, E. Ma, Y.T. Zhu, *Adv. Mater.* 18 (2006) 2280.
- [14] K.X. Tao, H. Choo, H.Q. Li, B. Clausen, J.E. Jin, Y.K. Lee, *Appl. Phys. Lett.* 90 (2007) 101911.
- [15] Y.B. Wang, J.C. Ho, Y. Cao, X.Z. Liao, H.Q. Li, Y.H. Zhao, E.J. Lavernia, S.P. Ringer, Y.T. Zhu, *Appl. Phys. Lett.* 94 (2009) 091911.
- [16] Y.B. Wang, B.Q. Li, M.L. Sui, S.X. Mao, *Appl. Phys. Lett.* 92 (2008) 011903.
- [17] Y.B. Wang, J.C. Ho, X.Z. Liao, H.Q. Li, S.P. Ringer, Y.T. Zhu, *Appl. Phys. Lett.* 94 (2009) 011908.
- [18] H. Van Swygenhoven, *Mater. Today* 9 (2006) 24.
- [19] H.Q. Li, F. Ebrahimi, *Mater. Sci. Eng. A* 347 (2003) 93.
- [20] A.P. Zhilyaev, T.G. Langdon, *Prog. Mater. Sci.* 53 (2008) 893.
- [21] Y. Cao, Y.B. Wang, S.N. Alhajeri, X.Z. Liao, W.L. Zheng, S.P. Ringer, T.G. Langdon, Y.T. Zhu, *J. Mater. Sci.* 45 (2010) 765.
- [22] G.K. Williamson, W.H. Hall, *Acta Metall.* 1 (1953) 22.
- [23] G.K. Williamson, R.E. Smallman, *Phil. Mag.* 1 (1956) 34.
- [24] R.E. Smallman, K.H. Westmacott, *Phil. Mag.* 2 (1957) 669.
- [25] V. Yamakov, D. Wolf, S.E. Phillpot, A.K. Mukherjee, H. Gleiter, *Nat. Mater.* 1 (2002) 45.
- [26] J. Schiøtz, K.W. Jacobsen, *Science* 301 (2003) 1357.
- [27] Z.W. Shan, R.K. Mishra, S.A. Syed Asif, O.L. Warren, A.M. Minor, *Nat. Mater.* 7 (2008) 115.
- [28] A.J. Haslam, S.R. Phillpot, D. Wolf, D. Moldovan, H. Gleiter, *Mater. Sci. Eng. A* 318 (2001) 293.
- [29] J.P. Hirth, J. Lothe, *Theory of Dislocations*, Krieger Publishing Co., Malabar, FL, 1992.